Electrochimica Acta 430 (2022) 141058

Contents lists available at ScienceDirect

Electrochimica Acta

journal homepage: www.journals.elsevier.com/electrochimica-acta

Investigating the V(IV)/V(V) electrode reaction in a vanadium redox flow battery – A distribution of relaxation times analysis

Monja Schilling, Michael Braig, Kerstin Köble, Roswitha Zeis *

Helmholtz Institute Ulm, Karlsruhe Institute of Technology, Helmholtzstraße 11, Ulm D-89081, Germany

ARTICLE INFO

Keywords:
Vanadium redox flow battery
Flow cell
Electrochemical impedance spectroscopy (EIS)
Distribution of relaxation times (DRT)
V(IV)/V(V) redox reaction

ABSTRACT

Due to the worldwide increasing energy demand and the urgency to act due to climate change, new energy storage technologies are required to balance the intermittent power supply of renewable energy sources. While the vanadium redox flow battery (VRFB) must still overcome lifetime and efficiency challenges, the technology is a promising candidate for large-scale energy storage. Thus, conducting experiments in a setup that closely mimics the operating conditions is vital for gaining new insights into the reactions and transport processes in a VRFB. We developed a novel 3D printed flow cell to study the individual half cell reactions of a VRFB under precisely controlled operating conditions. Using electrochemical impedance spectroscopy combined with the distribution of relaxation times analysis, we could identify the processes occurring in the half cell with the V(IV)/V(V) redox reaction by varying experimental parameters. We assigned peaks in different frequency ranges to the electrochemical reaction, the transport processes through the porous electrode structure, and the ion transport. This information is essential in the search for optimized operating conditions to improve the VRFB efficiency.

1. Introduction

Vanadium redox flow batteries (VRFBs) offer a promising concept for a large-scale energy storage solution to stabilize the electric grid and have gained increased attention over the last years [1–4]. Its design is highly flexible because the energy capacity and the power density are decoupled. However, this already commercially available battery type still faces challenges, such as reduced efficiency due to side reactions [1,5] or crossover [6], the solubility of the vanadium species in the electrolyte [7], the component degradation [5,8,9], and the need for improved cell architecture [10,11] and electrode materials [12–15]. The overall efficiency must be increased, and cell losses, including ohmic, kinetic, and transport losses, should be identified to render this technology more attractive for the commercial market. electrochemical impedance spectroscopy (EIS) presents a classical electrochemical technique to investigate these cell losses in battery and fuel cell research. EIS is non-destructive and often performed *in-situ* to identify and quantify the physicochemical processes within a cell, occurring on different time scales. It is possible to study a VRFB under operating conditions with a suitable setup [16–18].

Usually, impedance spectra are interpreted with an equivalent circuit model. However, a major challenge of this approach is the need for a priori knowledge about the system to choose an appropriate equivalent circuit [19–21]. Nevertheless, this data evaluation method is often used in VRFB research [22–24].

As another approach, the analysis of EIS data using the distribution of relaxation times (DRT) method can be beneficial since no assumptions or previous knowledge are necessary to analyze the data sets. In general, DRT analysis transforms the impedance data, a function of the frequency, into a distribution of time constants corresponding to the physical processes in the investigated system [16,25–28]. This method is already well known and commonly used in e.g., fuel cell [17,20,21,27–30] and Li-ion battery [16,31] research, but it is still a relatively new approach in VRFB research.

Tichter et al. [32] demonstrated that fundamental investigations with different carbon powder materials in a rotating ring-disk setup are possible. Their findings from standard techniques such as cyclic voltammetry were supported by EIS coupled with DRT analysis. The same group presented the first application of DRT analysis in a single cell VRFB [30]. They identified the faradaic process in the negative half cell of the VRFB and demonstrated that DRT analysis shows excellent potential for the characterization of VRFBs.

For the operation of a VRFB or the electrolyte rebalancing in the system, it is crucial to precisely know its State of Charge (SoC) in the half

* Corresponding author.
E-mail address: roswitha.zeis@kit.edu (R. Zeis).

https://doi.org/10.1016/j.electacta.2022.141058
Received 25 April 2022; Received in revised form 15 August 2022; Accepted 15 August 2022
Available online 16 August 2022

cells. Several different methods to determine the SoC have been presented, including the monitoring of the open circuit potential [33,34], the electrolyte conductivity [34], and the electrolyte density [33], or the use of spectrophotometric measurements [27,34,35]. Nevertheless, a significant disadvantage of these methods is that they require additional instruments. Thus, research groups seek a method that delivers accurate results while not requiring purchasing complex additional equipment.

This study investigates the electrochemical and transport processes during the V(IV)/V(V) redox reaction in a VRFB and utilizes the DRT analysis to gain new insights. Therefore, a novel 3D printed flow cell was developed to conduct experiments under well-defined measurement conditions. We assigned the corresponding peaks in the DRT spectra to the electrochemical reaction and different transport processes in the half cell by varying its operating parameters. This technique of coupling EIS measurements with DRT analysis was further utilized to determine the SoC of the electrolyte in the investigated half cell. In the future, this knowledge can be used to develop e.g., an equivalent circuit or a physics-based model for simulation or further data evaluation.

2. Experimental

2.1. Materials and electrolytes

SGL Carbon (Meitingen, Germany) supplied the carbon materials. The carbon felt SIGRACELL® GFA 6.0 EA and the carbon paper SIGRACET® GDL 39 AA were thermally pretreated as proposed in the literature to enhance the wettability and the electrochemical performance [36,37]. The carbon materials were placed in a covered glass petri dish and heated up to 400 °C for 25 h in a muffle furnace in an air atmosphere. Before assembling the cell, the carbon materials were immersed in ultrapure water (18.2 MΩcm) and sonicated for two minutes to remove contaminations and small fiber fragments from cutting.

Vanadium(IV) electrolyte was prepared by dissolving $VOSO_4$ (vanadyl sulfate hydrate, 99.9% metal basis, Thermo Fisher Scientific) in diluted H_2SO_4 (diluted from concentrated sulfuric acid, 96%, Suprapur®, Merck with ultrapure water (18.2 MΩcm)). 0.1 M VOSO4 in 2 M H_2SO_4 was chosen as a standard concentration.

Starting from the vanadium(IV) electrolyte, a charging procedure was performed to receive a vanadium(V) electrolyte using a VRFB in a redox flow test system (Scribner 857 Redox Flow Cell Test System, Scribner Associates Inc.). First, a constant current of 40 mA cm^{-2} was applied until a cut-off cell voltage of 1.8 V was reached. Second, a constant cell voltage of 1.8 V was applied until the current was lower than the cut-off current of 1 mA cm^{-2}.

2.2. Imaging of carbon materials

Images of the carbon materials were taken with a light microscope (AXIO Zoom.V16, Carl Zeiss Microscopy GmbH) to characterize the fiber arrangement. Scanning Electron Microscopy (SEM) images were conducted (LEO 1550 VP, Carl Zeiss AG, InLens detector, 3 keV acceleration voltage) for a more detailed visual analysis.

2.3. Experimental setup

The electrochemical measurements were performed with an in-house developed 3D printed flow cell (Fig. 1a), designed to ensure steady-state conditions during the experiment and to mimic the behavior of a commercial VRFB. The carbon material was placed directly in the flow channel in the bottom part of the cell to imitate the flow conditions in a commercial cell. The carbon material for the working electrode (WE)

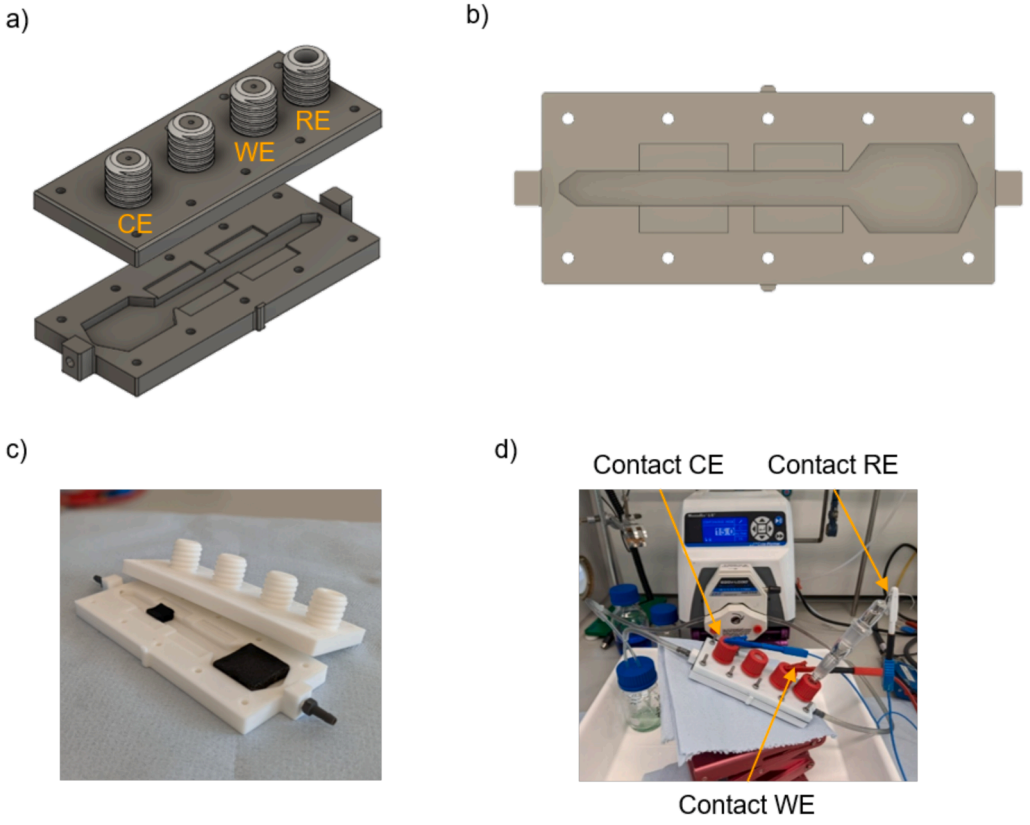

Fig. 1. Schematic display of (a) the in-house developed 3D printed flow cell highlighting the positions of the electrodes, (b) the bottom part of the cell, (c) picture of the cell with inserted carbon electrode material, and (d) picture of the experimental setup consisting of the assembled flow cell, the electrolyte reservoir, and the peristaltic pump.

was cut to a square piece of 1.0 x 1.0 cm and contacted by a 0.25 mm thick gold foil (99.9975 + %, Alfa Aesar). As the counter electrode (CE), another piece of carbon material (2.5 x 2.5 cm) was used, which was electrically contacted by a 1.0 mm thick titanium foil (99.2%, Alfa Aesar). Both metal foils were contacted with a gold wire of 0.5 mm diameter (99.9975 + %, Alfa Aesar). In the case of carbon paper, a stack of five pieces was used as the WE and/or the CE to ensure a certain volume for the electrolyte to flow through. An in-house developed hydrogen reference electrode was inserted as the reference electrode (RE; Fig. 1b). Since the compression rate of the electrode can influence the mass transport, a compression rate of 11% was used for the carbon paper, and a rate of 37% was used for the carbon felt. The cell was tightened using ten screws, which are fixed hand-tightened.

During the measurement, the electrolyte was pumped from the electrolyte reservoir through the flow cell and back to the reservoir by a peristaltic pump (Masterflex L/S®, Cole-Parmer), as displayed in Fig. 1b. Continuously pumping is required to ensure steady-state conditions since the conditions at the electrodes should not change to gain meaningful impedance data. For experiments at elevated temperatures, the electrolyte reservoir was placed in an oil bath, and the measurement was started after an equilibration period of 1.5 h.

2.4. Electrochemical impedance spectroscopy and data processing

The electrochemical measurements were performed with the previously described setup using an SP-300 potentiostat (BioLogic Science Instruments). The following parameters were varied independently: the carbon material, the flow rate, the temperature, the concentration of the vanadium species, the sulfuric acid concentration, the applied potential, and the SoC of the electrolyte. The standard EIS measurements were conducted at room temperature with carbon paper as the WE and the CE and a flow rate of 15 mL min^{-1}. The standard electrolyte consists of 0.1 M VO^{2+} in 2 M sulfuric acid. The standard measurements were performed in the potentiostatic mode in a frequency range from 100 kHz to 2 mHz with a single sinusoidal excitation of 5 mV as the perturbation and an applied potential of 1.05 V vs. RHE.

The Kramers-Kronig transform evaluated the data quality according to the standard procedure provided by Schönleber et al. [38,39]. The data were further analyzed using a MATLAB-based tool called DRTtools [25] based on the Tikhonov regularization. The spectra fitting is based on a Gaussian function for the discretization and includes the inductive data. As a regularization parameter, 1E-9 was chosen. The influence of the regularization parameter is demonstrated in Fig. 12 (supporting information).

3. Results and discussion

This section will first demonstrate the quality check of the EIS data by Kramers-Kronig transform. Second, we will propose the peak assignments of the DRT spectrum, which were obtained by varying different parameters independently. These assignments are explained and discussed in further detail in the following sections.

3.1. Validity check of the measured EIS data

The measured EIS data must fulfill high-quality standards to ensure the validity of the DRT analysis. Therefore, the Kramers-Kronig transform was performed to check the data quality. A typical result for such a validity check is shown in Fig. 2. Since all measured residuals are smaller than 1%, the data are reliable and can be analyzed with DRTtools [16, 17].

3.2. General assignments of the peaks in the DRT spectra

DRT analysis was used to separate the individual processes in the half cell of the V(IV)/V(V) redox reactions and assign a frequency corresponding to a time constant to each process. Fig. 3 displays a typical spectrum for the setup and gives an overview of the peak assignments to the half cell processes. The DRT spectrum displays the distribution function of the relaxation times γ(f) against the frequency. A general color code for the three specific frequency ranges provides a better understanding of the spectrum. The DRT analysis reveals one smaller peak in the high-frequency range above 50 Hz (yellow), which corresponds to the electrochemical redox reaction between vanadium(IV) and vanadium(V). In the mid-frequency range between 10 mHz and 50 Hz (green), several peaks are observed, which were assigned to the transport processes of the active redox species through the porous structure of the carbon electrode. Furthermore, we attributed the vanadium ion transport to the single peak in the low-frequency range below 10 mHz (blue). These assignments will be justified in the following sections.

3.3. Influence of the carbon material

Measurements with different electrode materials were performed to investigate the influence of the WE and the CE on the EIS and DRT spectra. A stack of carbon paper (CP) or a carbon felt (CF) was implemented into the flow cell setup. Fig. 4 displays images of these materials with different magnifications using different visualization techniques. They show that the CF (Fig. 4a–c) is significantly thicker than the CP (Fig. 4d-f), has a higher porosity (open porosity of CF: 95% [40] versus CP: 89% [41]), and a disordered fiber arrangement. The CP is fabricated from chopped fibers and glued together with a binder to produce thin

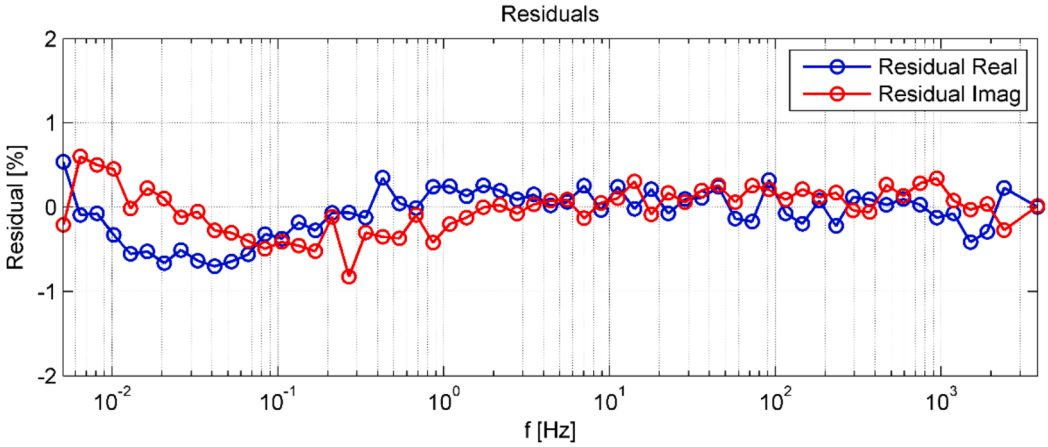

Fig. 2. Typical result for a quality check of measured EIS data using Kramers-Kronig transform.

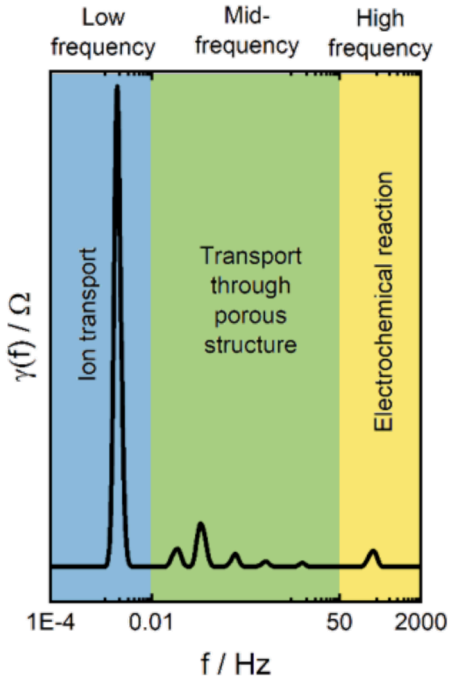

Fig. 3. Schematic display of the proposed peak assignments to the half cell processes using an exemplary DRT spectrum.

sheets. Thus, this material contains fewer voids or pores. The different morphology of the CF and the CP significantly affect the flow-through behavior of the electrolyte [14,28,42] and, consequently, the impedance response of the cell.

The Nyquist plots measured with different carbon materials as the WE and the CE and the corresponding DRT spectra are presented in Fig. 5. The impedance spectra differ significantly in both shape and size. When the CF was utilized as the WE and the CE (Fig. 5, black curve), the Nyquist plot displays only a small semicircle in the high-frequency range and one suppressed and elongated semicircle at lower frequencies. Using DRT analysis, the superimposed semicircles were separated into several peaks. One small peak was observed at a high frequency (over 50 Hz), and several peaks are visible in the mid-frequency range (10 mHz to 50 Hz). The mid-frequency peaks contribute the largest share to the overall impedance.

When the WE was replaced by a stack of CP (Fig. 5, red curve), the Nyquist plot's shape and the corresponding DRT spectrum altered significantly. Furthermore, the overall impedance decreased, mainly due to the lower impedance in the mid-frequency range of the DRT spectrum. The Nyquist plot in this electrode configuration (WE = CP, CE = CF) shows a small semicircle in the high-frequency range. In addition, a slightly suppressed semicircle is measured in the mid-frequency range, which merges into another larger semicircle at low frequencies. Here, only the onset of the low-frequency semicircle is visible since the measurement was terminated to avoid long acquisition times. Furthermore, a straight vertical line below the x-axis is observed in the high-frequency range, attributed to the inductance of the cabling and the gold wires used to contact the electrode. This artifact can be observed in all measurements and is therefore independent of the choice of material.

The shape of the Nyquist plot with CP as the WE and the CE (Fig. 5, green curve) is similar to the previous electrode configuration. The vertical straight line merges into a small semicircle at high frequency, which merges into another semicircle. This semicircle is significantly smaller than the previous measurement with the CF as the CE. Again, only the onset of a third semicircle is measured in the low-frequency range. The overall impedance of this configuration is slightly decreased since using CP instead of CF in the CE position lowers the impedances in the mid-frequency range.

Since the fiber arrangements of the material – especially at the WE – influence the observed peaks in the mid-frequency range significantly, we concluded that the transport processes cause the impedances in the mid-frequency range of the DRT spectra through the porous structure of the carbon electrode. Therefore, this feature of the DRT spectrum – the electrode material's fingerprint – can be used to probe the material's morphology and wettability. In the subsequent experiments, we chose carbon paper as the WE and the CE to investigate other aspects of the

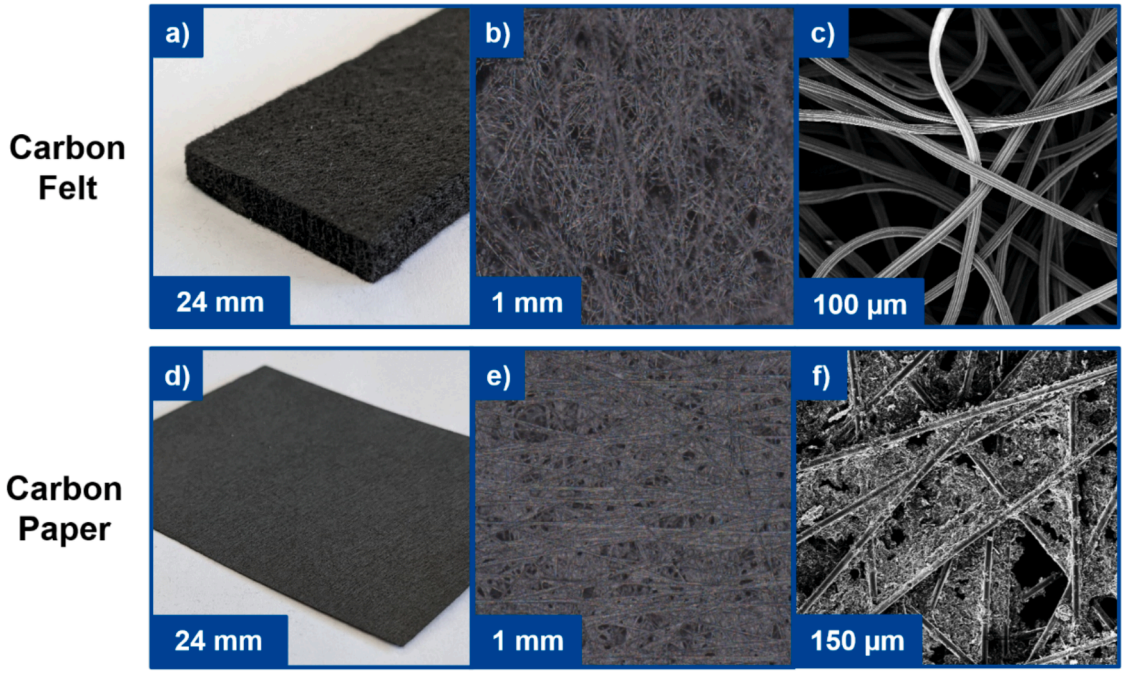

Fig. 4. Displays of the carbon materials' fiber arrangements and structure: (a)/(d) a picture, (b)/(e) a light microscope image (32x magnification), and (c)/(f) an SEM image of the CF/the CP.

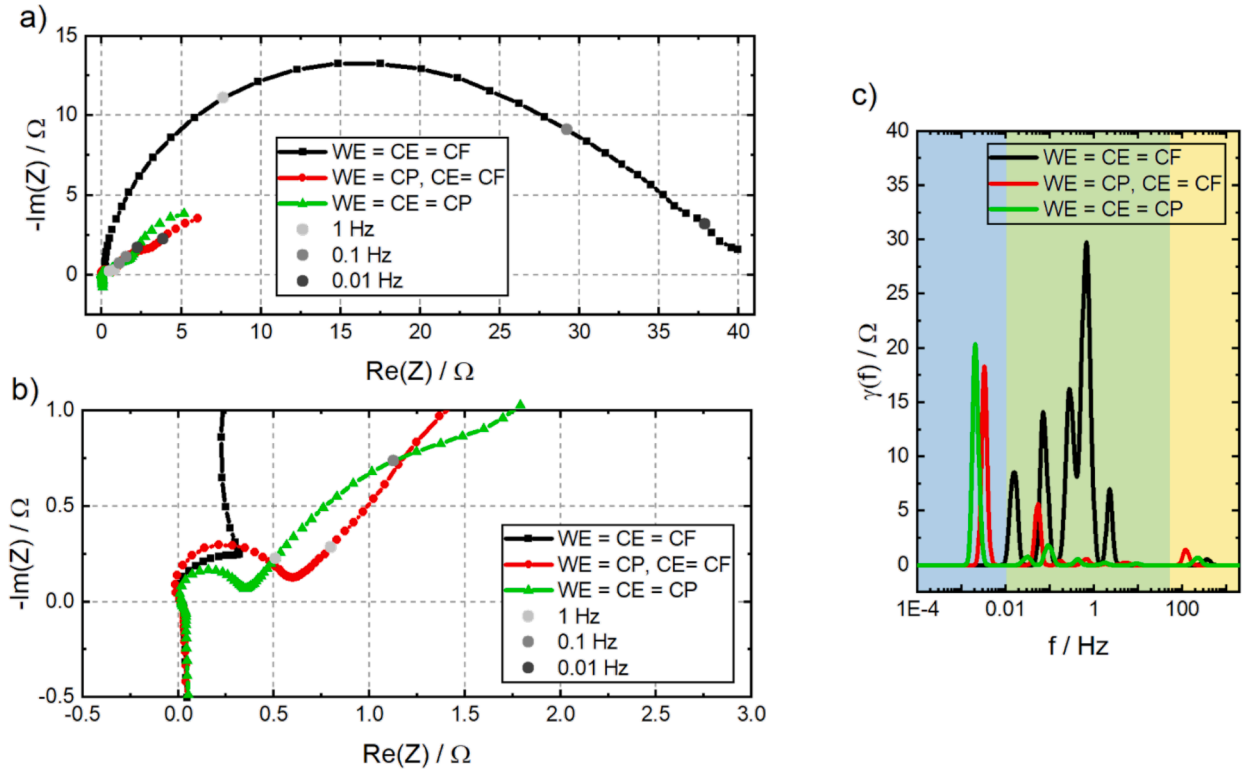

Fig. 5. (a) Nyquist plots, (b) enlarged section of the high frequency range of the Nyquist plot, and (c) corresponding DRT spectra of different electrode combinations using CF and/or CP. All measurements were performed at room temperature in the standard vanadium(IV) electrolyte with a flow rate of 20 mL min^{-1}.

DRT spectrum since the impedance due to the electrode's structure should not dominate it.

3.4. *Influence of the flow rate*

Fig. 6 shows the Nyquist plots and DRT spectra at different flow rates utilizing CP as the WE and the CE.

A higher flow rate mainly alters the arc at low frequencies associated with the transport of vanadium species through the aqueous electrolyte. However, it leaves the mid-frequency range almost and the high-frequency range generally unaffected, as shown in the Nyquist plots.

The DRT spectra show that the position of the single high-frequency peak at around 250 Hz is fixed, and the peak area is equivalent at all measured flow rates. According to experiments with fuel cells and other electrochemical devices, this high-frequency peak is linked to electrode reaction kinetics [16,43,44], corresponding to the electrochemical vanadium(IV) oxidation in this case. The variation of the flow rate does not influence this process.

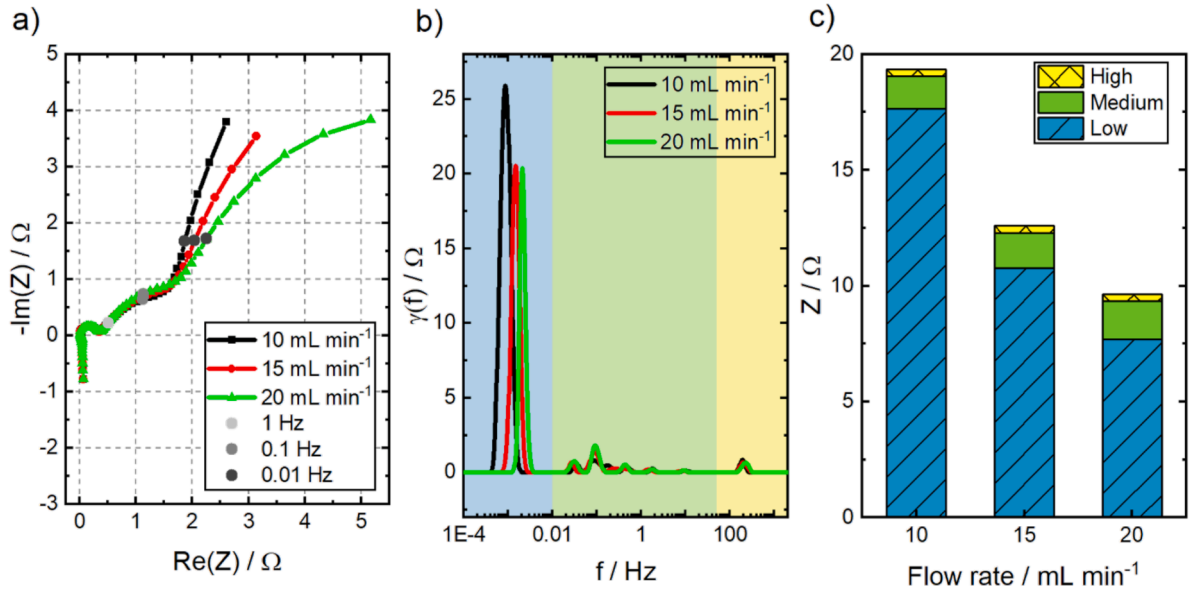

Fig. 6. (a) Nyquist plots and (b) corresponding DRT spectra at different flow rates of 10, 15, and 20 mL min^{-1}. (c) Display of the absolute impedance values in the specific frequency ranges. All measurements were performed at room temperature in the standard vanadium(IV) electrolyte with CP as the WE and the CE.

Several small peaks are visible in the DRT spectra in the mid-frequency range, which slightly increases with a higher flow rate. We assigned these peaks to the transport processes through the porous structure of the electrode in the previous section. The electrolyte is pumped faster through the flow cell and the electrodes at a higher flow rate. Therefore, the electrochemically active species in the electrolyte have less time to invade the electrode's pores, increasing the impedance of this process. The effect is marginal since the CP used as the WE is only 280 μm thick [41].

A higher flow rate is particularly beneficial for transporting the vanadium species through the electrolyte. Hence, we observe a lower impedance and a shift towards higher frequencies (Fig. 6b and c) for the low-frequency peak at around 10 mHz. This observation supports the proposed assignment of this peak to the ion transport through the electrolyte.

The same features described previously are observed in the Nyquist plots and DRT spectra of the other electrode material combinations (Fig. 13, supporting information). These experiments demonstrate that selecting the optimal electrode material for VRFBs is crucial to minimizing cell losses and, thus, increasing the overall efficiency. The presented method is a powerful tool to evaluate the flow properties of the porous materials and, therefore, specifically helpful in developing novel electrodes.

3.5. Influence of the vanadium(IV) and the sulfuric acid concentration

Since commercially available VRFBs are operated at high molar vanadium and sulfuric acid concentrations, different concentrations of the vanadium(IV) species or the sulfuric acid in the electrolyte were investigated and compared to our standard electrolyte composition (0.1 M VO^{2+} in 2 M H_2SO_4). The results are shown in the bar charts in Fig. 7. The respective Nyquist plots and DRT spectra of these measurements are attached in the supporting information (Fig. 15).

The peak in the high-frequency range, corresponding to the electrochemical reaction, is not affected by varying the vanadium(IV) ion or the sulfuric acid concentration. The sulfuric acid concentration does not influence the electrochemical reaction, and the concentration of the vanadium reactant should not influence the reaction mechanism, including the rate-determining step, in this small range of concentrations [45]. Therefore, the peak position and the impedance of this process remain constant when varying the concentrations.

The ion transport in sulfuric acid and the transport through the porous network benefit from more electrochemically active species in the electrolyte due to decreased transport distances. Increasing the vanadium(IV) concentration shows a significant impedance decrease in the low- and mid-frequency range. Specifically, the impact on the ion transport process at low frequency is significant and demonstrates that operating a VRFB with a high molar electrolyte is essential.

The bar chart in Fig. 7b, summarizes the impact of the sulfuric acid concentration on the cell impedance. A higher sulfuric acid concentration in the electrolyte increases its viscosity [46,47], which hampers the vanadium ion transport and consequently causes this transport process to be the dominating share of the total cell impedance. Zhao et al. studied the impact of the sulfuric acid concentration and noticed an increase in the viscosity from 3.03 $mm^2\ s^{-1}$ at 1.5 M sulfuric acid to 4.54 $mm^2\ s^{-1}$ at 4.0 M sulfuric acid concentration [47]. Additionally, we observed that the respective low-frequency peak shifts to even lower frequencies with rising viscosity (Fig. 15, supporting information). In contrast, the impedances related to the mid-frequency range first decrease with rising sulfuric acid concentration and later increase again. We propose that two contrary effects cause this relation. With an increasing sulfuric acid concentration, the electrolyte shows a more substantial oxidizing effect; thus, the carbon material's surface functional groups are altered. This effect also leads to a different wetting behavior, which is enhanced with higher concentrations since the impedances are decreasing [48,49]. Nevertheless, if the sulfuric acid concentration is very high (e.g., 4 M), the increased viscosity of the electrolyte counterbalances this effect, and the mid-frequency impedance rises again.

In conclusion, high molar vanadium(IV) concentrations are beneficial, but a high viscosity due to high sulfuric acid concentrations reduces the VRFB efficiency. Therefore, the ideal operating condition would be high vanadium concentrations in highly diluted sulfuric acid.

3.6. Influence of the operating temperature

This section presents the influence of the operating temperature on the Nyquist plot and the DRT spectrum (Fig. 8).

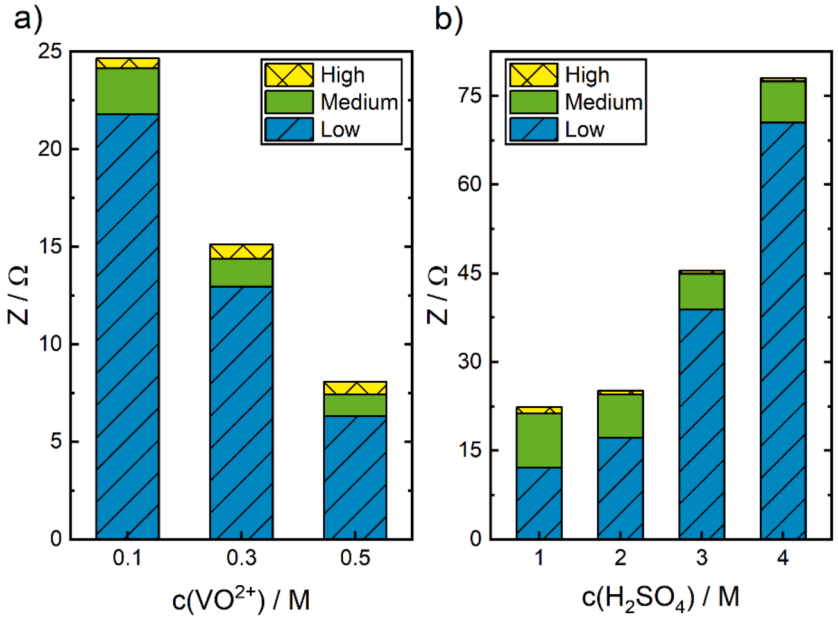

Fig. 7. Influence of (a) the vanadium(IV) and (b) the sulfuric acid concentration in the electrolyte on the impedances of the three frequency ranges. A solution of 0.1 M $VOSO_4$ in 2 M H_2SO_4 was used as starting point at room temperature with CP as WE and CE (15 mL min^{-1} flow rate).

The operating temperature affects all three frequency ranges of the Nyquist plot and the corresponding DRT spectrum. The high-frequency peak in the DRT spectrum decreases significantly at higher temperatures. The vanadium(IV) oxidation rate constant is temperature-dependent [50]. At higher temperatures, the reactants have higher internal energy and are more likely to overcome the activation barrier of the electrochemical reaction. Thus, the impedance of this process decreases. At the same time, the peak frequency remains constant, implying that the process's time constant does not change. Thus, the reaction mechanism and the rate-determining step are independent of the temperature.

The decreased electrolyte viscosity and thus also influenced mass diffusivity due to higher operating temperatures promote the transport processes in the mid-and low-frequency range. The vanadium ions can be transported more easily and quickly through a less viscous electrolyte resulting in a higher mass diffusivity, which causes the impedance of the ion transport and the transport through the porous structure to decrease significantly. Simultaneously, the increased temperature of the electrolyte changes the wettability of the electrolyte towards the electrode. At the same time, the peak position of the ion transport process is constant.

3.7. Influence of the vanadium species and the electrochemical reaction

In the half cell of the V(IV)/V(V) redox reactions, only vanadium(IV) is present when the battery is fully discharged, and only vanadium(V) ions are present in the fully charged state. The vanadium(IV) oxidation or vanadium(V) reduction is kinetically favored depending on the applied potential. This section investigated the impacts of the oxidation state and the occurring electrochemical reaction.

So far, all experiments have been performed in vanadium(IV) electrolyte at a potential of 1.05 V vs RHE, which corresponds to the onset of the vanadium(IV) oxidation peak in a cyclic voltammogram. However, if we want to use pure vanadium(V) electrolyte, the applied potential should favor the opposite reaction – the vanadium(V) reduction. Cyclic voltammetry was performed in the three-electrode setup to ensure that the negative current response at the chosen vanadium(V) reduction potential matches the positive current response at 1.05 V vs. RHE (Fig. 14 in the supporting information). The positive current at 1.05 V vs. RHE was determined from this measurement, and the potential corresponding to the respective negative current value was identified as 1.10 V vs RHE. Thus, this potential was used for the following EIS measurements with pure vanadium(V) electrolytes. The EIS and DRT spectra of the two solutions with different vanadium oxidation states are displayed in Fig. 9.

It must be noted that more frequency points were measured for the vanadium(V) electrolyte to prove the finiteness of the data, which is a requirement to perform an accurate DRT analysis. The DRT analysis can be applied since the Nyquist plot indicates partial semicircles at lower frequencies.

In the cell, different reaction types are favored due to various applied potentials and electrolytes. Surprisingly, the high-frequency peak appears at a similar frequency (around 200 Hz) in both measurements, and the corresponding impedances of the vanadium(IV) oxidation (313 mΩ) and the vanadium(V) reduction (324 mΩ) are very similar. Since the peak positions are almost equal, the rate-determining step in both reactions must be equally fast.

In the low-frequency range, the peak of the ion transport process is influenced by the electrolyte species. In the vanadium(V) electrolyte, the peak appears at a higher frequency (2.6 mHz) compared to the measurement in the vanadium(IV) electrolyte (1.5 mHz). Since the vanadium(V) electrolyte has a lower viscosity than the vanadium(IV) electrolyte and thus, the mass diffusivity is influenced [48,51]. This relation between the frequency of the process and the viscosity of the electrolyte solution and mass diffusivity is similar to the previous results with different sulfuric acid concentrations (Fig. 15, supporting information). Therefore, the ion transport process is faster in vanadium(V) electrolyte, and the corresponding peak shifts to a higher frequency.

3.8. Influence of the applied potential

It was necessary to choose an appropriate potential for both experiments to perform the previously presented measurements with different vanadium electrolytes. The following section will discuss the influence of the applied potential on the EIS and DRT spectra using pure vanadium (V) electrolyte. The same measurement procedure with vanadium(IV) electrolyte is presented in the supporting information (Fig. 16).

The vanadium(V) electrolyte used in the presented measurements has an open circuit potential of 1.169 V vs RHE. The applied potential should be below this value to shift the reaction equilibrium towards the vanadium(V) reduction. Therefore, potentials between 1.10 V vs RHE

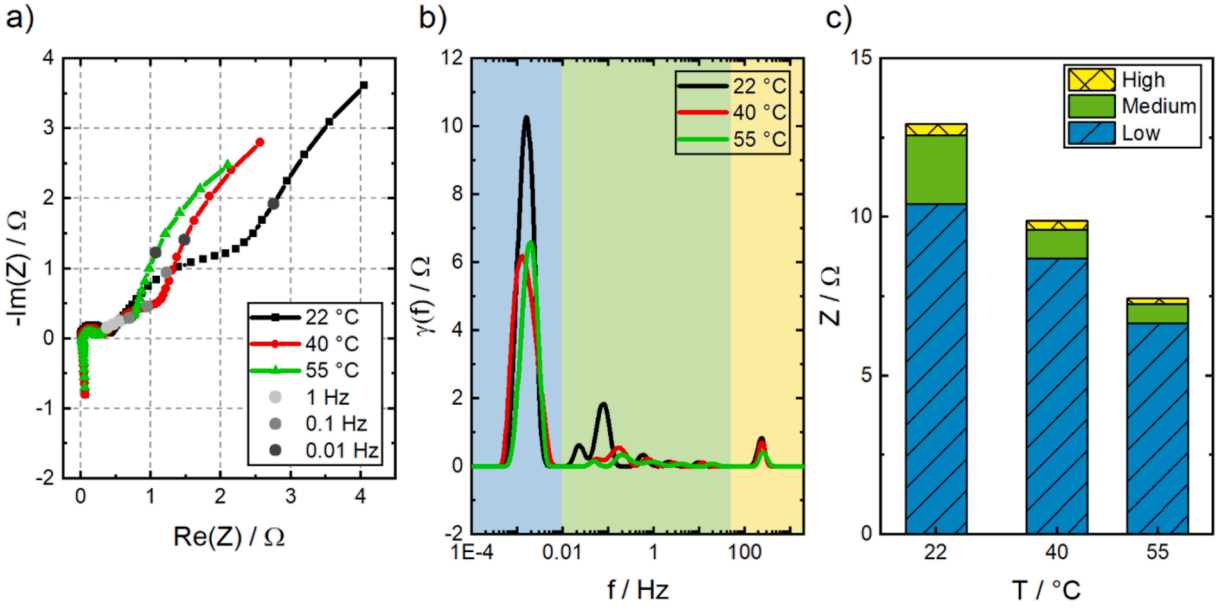

Fig. 8. (a) Nyquist plots and (b) corresponding DRT spectra at different operating temperatures. (c) Display of the absolute impedance values in the specific frequency ranges. All measurements were performed at a constant flow rate of 15 mL min^{-1} in the standard vanadium(IV) electrolyte with CP as the WE and the CE.

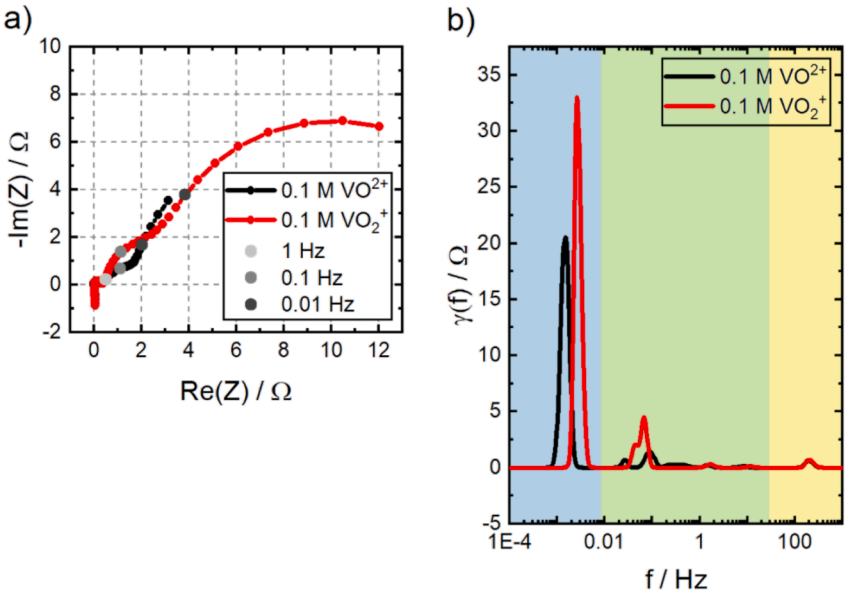

Fig. 9. (a) Nyquist plots and (b) corresponding DRT spectra measured in pure vanadium(IV) or vanadium(V) electrolyte with a concentration of 0.1 M VO^{2+} or VO_2^+ in 2 M H_2SO_4. All measurements were performed at room temperature at a constant flow rate of 15 mL min^{-1} with CP as the WE and the CE.

and 1.16 V vs RHE were applied in the following EIS measurements presented in Fig. 10. The corresponding DRT spectra show that the peak at high frequencies, which corresponds to the electrochemical reaction, is not affected by the applied potential. Therefore, the electrochemical reaction and the reaction mechanism must remain the same.

In contrast, the change in applied potential influences the peaks in the low- and medium-frequency range. The impedances related to both ranges decrease with decreasing potential. Applying different potentials in the potential range of the electrochemical reaction alters the double layer of the electrode. Since the electrostatic forces at the electrode-electrolyte interface define the vanadium ions' concentration distribution, the double layer change caused by the applied potentials impacts the impedances in the low- and medium-frequency ranges. The apparent effect on the impedance of the low-frequency peak is shown in Fig. 10c. Reducing the potential from 1.16 V to 1.10 V vs RHE causes the low-frequency impedance to drop six times.

In conclusion, the choice of the applied potential significantly influences the triggered processes in the half cell of the V(IV)V(V) redox reactions, as observable in the measured Nyquist plots and the resulting DRT spectra. Thus, the choice of the applied potential is crucial. The following section will present an approach for choosing the cell potential for investigations of the SoC.

3.9. *Influence of the state of charge*

An important parameter to consider when analyzing the half cell processes of a VRFB is the SoC of the electrolyte. During the operation of a VRFB, the SoC will continuously change due to redox reactions taking

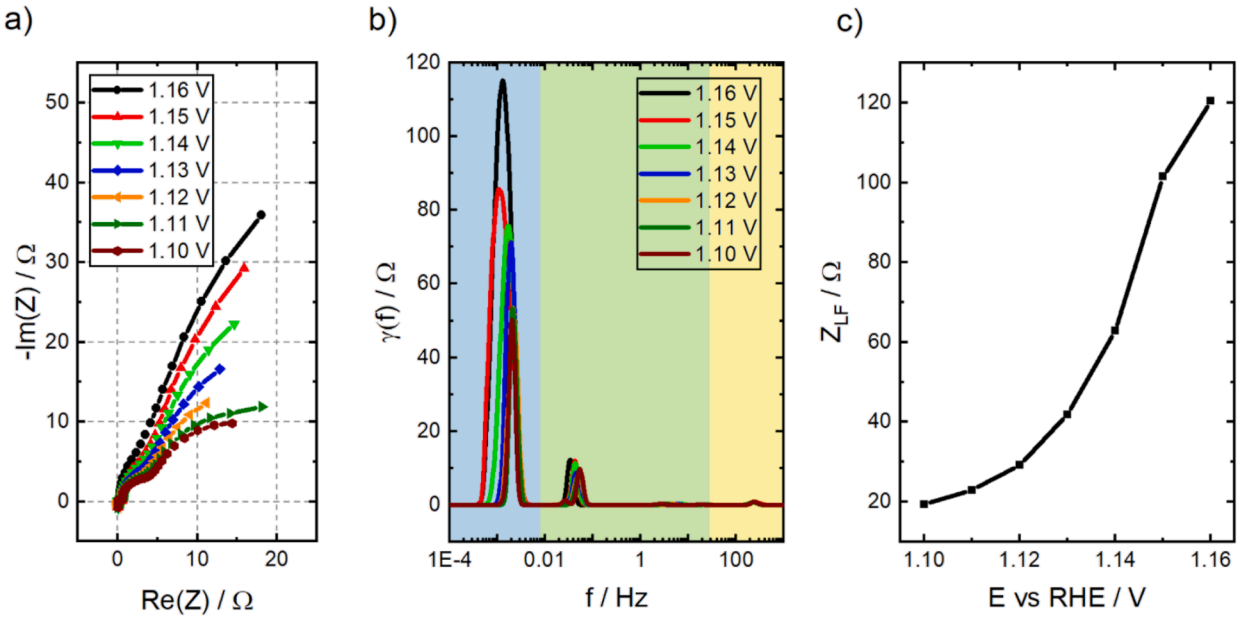

Fig. 10. (a) Nyquist plots and (b) corresponding DRT spectra at different applied potentials. (c) Influence of the applied potential on the impedance of the low-frequency peak. All measurements were performed at a constant flow rate of 15 mL min^{-1} in 0.1 M VO_2^+ in 2 M H_2SO_4 with CP as the WE and the CE.

place. Defined volumes of vanadium(IV) and vanadium(V) electrolyte were mixed to mimic an intermediate SoC of the battery. After an equilibration time of 10 min, the flow cell's open circuit potential (E_{oc}) was determined. The applied potentials for the EIS measurements were selected according to the protocol presented in Fig. 11b, which implies adding or subtracting 50 mV to the measured E_{oc}. This measure ensures well-defined operating conditions and only causes minor faradaic currents, which will not alter the SoC of the electrolyte. Furthermore, side reactions or undesired reactions during the measurement can be prevented if only a slight deviation from the E_{oc} is chosen. Nevertheless, higher potential deviations have been tested, and the results of these experiments are presented in the supporting information (Fig. 17). Using a higher potential than the E_{oc}, the preferred reaction is the vanadium (IV) oxidation to vanadium(V). The vanadium(V) reduction to vanadium(IV) is more likely to occur if a potential lower than the E_{oc} is applied.

This section presents a novel approach to determining the SoC of the electrolyte in the half cell of the V(IV)/V(V) redox reactions based on EIS measurements and DRT analysis. In the DRT spectra of the electrolytes with different SoC values, we observed that the impedance of the low-frequency peak (Z_{LF}) strongly correlates to the SoC of the electrolyte (Fig. 11c). Thus, a simple EIS measurement in combination with DRT analysis can be used to determine the SoC of the vanadium electrolyte.

The impedance related to the low-frequency peak (Z_{LF}) is obtained using DRT analysis. The value corresponds to the area under the graph of the peak. The impedance increases with increasing SoC for the measurements at a potential of E_{oc} + 50 mV. The E_{oc} − 50 mV measurements show the opposite trend as the impedance decreases with higher SoC. However, the 0 and 100% SoC measurements do not fit the trends and are excluded in the following discussion. In short, the impedance decreases if more reactants are available for the reaction favored by the applied potential. As an example: if a higher potential than the E_{oc} is applied, the vanadium(IV) ions are oxidized. If the SoC of the electrolyte is low, many vanadium(IV) ions are present and can be oxidized. Thus, the impedance related to the low-frequency peak is low. In contrast, a high SoC corresponds to a low concentration of vanadium(IV) ions in the electrolyte. A potential higher than the E_{oc} leads in this case to a high low-frequency impedance. For the reduction reaction (applying a potential below E_{oc}), the same behavior is observed. The proposed method to determine the SoC is particularly beneficial for the mid-range SoC values of a battery. In this range, the E_{oc} only differs slightly for different SoC values; thus, the SoC determination via the E_{oc} is less accurate.

In conclusion, a combination of open circuit potential monitoring (for low and high SoC values) and the EIS-based method (for mid-range SoC values) improves the accuracy of the SoC determination of vanadium electrolytes. A random SoC of 66% was chosen, and the respective electrolyte solution was mixed to test our EIS-based approach. In Fig. 11c, the impedances of its low-frequency peak, measured at E_{oc} + 50 mV and E_{oc} − 50 mV, are highlighted green. Both impedance values match the results of the previous SoC measurements and confirm the reported relationship between the SoC of the electrolyte and the low-frequency impedance. This experiment shows that a potentiostat combined with a frequency response analyzer can be used to monitor the SoC of the vanadium electrolyte during the charging and discharging of a VRFB.

4. Conclusion

EIS data of the electrochemical V(IV)/V(V) redox reactions were analyzed utilizing the DRT tool. The experiments were conducted with a

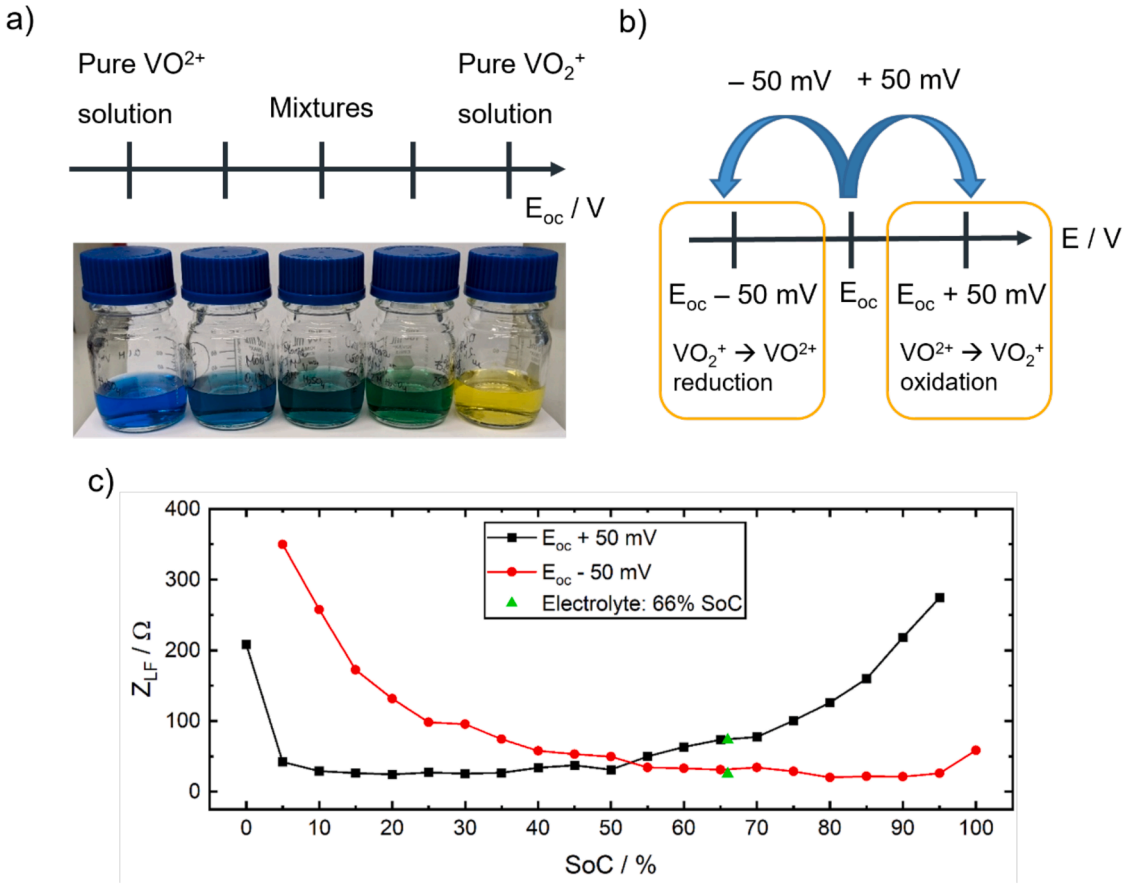

Fig. 11. (a) Picture of vanadium electrolytes with different SoC values, (b) scheme of the choice of applied potentials during EIS measurements using electrolytes with different SoC, and (c) relation between the impedance of the low-frequency peak and the SoC of the vanadium electrolyte.

3D printed flow cell to ensure controlled operating conditions. Several parameters were varied, including the carbon electrode material used as the WE and/or the CE, the flow rate, the vanadium(IV) and the sulfuric acid concentration, the temperature, the oxidation state of the vanadium ions, the applied potential, and the SoC of the electrolyte to separate and identify individual impedance contributions of the cell. This approach allowed us to assign the various peaks in the DRT spectrum to specific reaction and transport processes in the cell.

The peak in the high-frequency range above 50 Hz is related to the electrochemical reaction of the vanadium species in the electrolyte. Several peaks in the mid-frequency range between 10 mHz and 50 Hz are linked to the electrolyte transport processes through the porous electrode structure and can be seen as a fingerprint of the electrode material. The single peak in the low-frequency range below 10 mHz corresponds to the ion transport.

This study was able to assign peaks to individual processes. In the future, this knowledge can be used to develop e.g., an equivalent circuit or a physics-based model, which can also be used for simulations or further data evaluation, including extracting relevant metrics such as rate constants or mass transfer rates.

Based on this study, it is beneficial to operate a VRFB at higher flow rates, at elevated temperatures, with a high concentration of vanadium (IV) ions and a low sulfuric acid concentration to minimize the impedances of the individual processes.

This advanced characterization technique helps find optimal operating conditions and select suitable porous electrode materials to increase the battery's efficiency. Furthermore, it can electrochemically determine the SoC of the vanadium electrolyte without additional equipment.

CRediT authorship contribution statement

Monja Schilling: Visualization, Formal analysis, Data curation, Investigation, Methodology, Writing – original draft. **Michael Braig:** Formal analysis, Methodology, Writing – review & editing. **Kerstin Köble:** Methodology, Writing – review & editing. **Roswitha Zeis:** Conceptualization, Funding acquisition, Supervision, Writing – review & editing.

Declaration of Competing Interest

The authors declare that they have no known competing financial interests or personal relationships that could have appeared to influence the work reported in this paper.

Data Availability

Data will be made available on request.

Acknowledgments

We especially thank Felix Matzik, Ulm University, Institute of Electrochemistry, for manufacturing the 3D printed flow cells and SGL Carbon for supplying the SIGRACELL® carbon felts and the SIGRACET® carbon paper. This work contributes to the research performed at CELEST (Center for Electrochemical Energy Storage Ulm-Karlsruhe).

Supplementary materials

Supplementary material associated with this article can be found, in the online version, at doi:10.1016/j.electacta.2022.141058.

References

[1] K. Lourenssen, J. Williams, F. Ahmadpour, R. Clemmer, S. Tasnim, Vanadium redox flow batteries: a comprehensive review, J. Energy Storage 25 (2019), 100844, https://doi.org/10.1016/j.est.2019.100844.
[2] K.J. Kim, M.S. Park, Y.J. Kim, J.H. Kim, S.X. Dou, M. Skyllas-Kazacos, A technology review of electrodes and reaction mechanisms in vanadium redox flow batteries, J. Mater. Chem. A 3 (2015) 16913–16933, https://doi.org/10.1039/C5TA02613J.
[3] M. Skyllas-Kazacos, M. Rychcik, R.G. Robins, A.G. Fane, M.A. Green, New all-vanadium redox flow cell, J. Electrochem. Soc. 133 (1986) 1057–1058, https://doi.org/10.1149/1.2108706.
[4] M. Skyllas-Kazacos, M.H. Chakrabarti, S.A. Hajimolana, F.S. Mjalli, M. Saleem, Progress in flow battery research and development, J. Electrochem. Soc. 158 (2011) R55, https://doi.org/10.1149/1.3599565.
[5] L. Eifert, Z. Jusys, R.J. Behm, R. Zeis, Side reactions and stability of pre-treated carbon felt electrodes for vanadium redox flow batteries: a DEMS study, Carbon 158 (2020) 580–587, https://doi.org/10.1016/j.carbon.2019.11.029. N Y.
[6] T. Lemmermann, M. Becker, M. Stehle, M. Drache, S. Beuermann, M.S. Bogar, U. Gohs, U.E. Fittschen, T. Turek, U. Kunz, *In situ* and in operando detection of redox reactions with integrated potential probes during vanadium transport in ion exchange membranes, J. Power Sources 533 (2022), 231343, https://doi.org/10.1016/j.jpowsour.2022.231343.
[7] M. Skyllas-Kazacos, L. Cao, M. Kazacos, N. Kausar, A. Mousa, Vanadium electrolyte studies for the vanadium redox battery-a review, ChemSusChem 9 (2016) 1521–1543, https://doi.org/10.1002/cssc.201600102.
[8] L. Eifert, Z. Jusys, R. Banerjee, R.J. Behm, R. Zeis, Differential electrochemical mass spectrometry of carbon felt electrodes for vanadium redox flow batteries, ACS Appl. Energy Mater. 1 (2018) 6714–6718, https://doi.org/10.1021/acsaem.8b01550.
[9] L. Gubler, Membranes and separators for redox flow batteries, Curr. Opin. Electrochem. 18 (2019) 31–36, https://doi.org/10.1016/j.coelec.2019.08.007.
[10] M. Al-Yasiri, J. Park, A novel cell design of vanadium redox flow batteries for enhancing energy and power performance, Appl. Energy 222 (2018) 530–539, https://doi.org/10.1016/j.apenergy.2018.04.025.
[11] D.S. Aaron, Q. Liu, Z. Tang, G.M. Grim, A.B. Papandrew, A. Turhan, T. A. Zawodzinski, M.M. Mench, Dramatic performance gains in vanadium redox flow batteries through modified cell architecture, J. Power Sources 206 (2012) 450–453, https://doi.org/10.1016/j.jpowsour.2011.12.026.
[12] S. Rümmler, M. Steimecke, S. Schimpf, M. Hartmann, S. Förster, M. Bron, Highly Graphitic, Mesoporous carbon materials as electrocatalysts for vanadium redox reactions in all-vanadium redox-flow batteries, J. Electrochem. Soc. 165 (2018) A2510–A2518, https://doi.org/10.1149/2.1251810jes.
[13] M. Steimecke, S. Rümmler, N.F. Schuhmacher, T. Lindenberg, M. Hartmann, M. Bron, A comparative study of functionalized high-purity carbon nanotubes towards the V(IV)/V(V) redox reaction using cyclic voltammetry and scanning electrochemical microscopy, Electroanalysis 29 (2017) 1056–1061, https://doi.org/10.1002/elan.201600614.
[14] J. Hereijgers, J. Schalck, T. Breugelmans, Mass transfer and hydrodynamic characterization of structured 3D electrodes for electrochemistry, Chem. Eng. J. 384 (2020), 123283, https://doi.org/10.1016/j.cej.2019.123283.
[15] C.T.C. Wan, D. López Barreiro, A. Forner-Cuenca, J.W. Barotta, M.J. Hawker, G. Han, H.C. Loh, A. Masic, D.L. Kaplan, Y.M. Chiang, F.R. Brushett, F.J. Martin-Martinez, M.J. Buehler, Exploration of biomass-derived activated carbons for use in vanadium redox flow batteries, ACS Sustain. Chem. Eng. 8 (2020) 9472–9482, https://doi.org/10.1021/acssuschemeng.0c02427.
[16] M.A. Danzer, Generalized distribution of relaxation times analysis for the characterization of impedance spectra, Batteries 5 (2019) 53, https://doi.org/10.3390/batteries5030053.
[17] A. Weiß, S. Schindler, S. Galbiati, M.A. Danzer, R. Zeis, distribution of relaxation times analysis of high-temperature PEM fuel cell impedance spectra, Electrochim. Acta 230 (2017) 391–398, https://doi.org/10.1016/j.electacta.2017.02.011.
[18] V.F. Lvovich, Impedance Spectroscopy: Applications to Electrochemical and Dielectric Phenomena, Wiley, Hoboken, N.J, 2012.
[19] N. Bevilacqua, T. Asset, M.A. Schmid, H. Markötter, I. Manke, P. Atanassov, R. Zeis, Impact of catalyst layer morphology on the operation of high temperature PEM fuel cells, J. Power Sources Adv. 7 (2021), 100042, https://doi.org/10.1016/j.powera.2020.100042.
[20] N. Bevilacqua, R.R. Gokhale, A. Serov, R. Banerjee, M.A. Schmid, P. Atanassov, R. Zeis, Comparing novel PGM-free, platinum, and alloyed platinum catalysts for HT-PEMFCs, ECS Trans. 86 (2018) 221–229, https://doi.org/10.1149/08613.0221ecst.
[21] A. Leonide, V. Sonn, A. Weber, E. Ivers-Tiffée, Evaluation and modeling of the cell resistance in anode-supported solid oxide fuel cells, J. Electrochem. Soc. 155 (2008) B36, https://doi.org/10.1149/1.2801372.
[22] T. Haisch, H. Ji, C. Weidlich, Monitoring the state of charge of all-vanadium redox flow batteries to identify crossover of electrolyte, Electrochim. Acta 336 (2020), 135573, https://doi.org/10.1016/j.electacta.2019.135573.
[23] C.N. Sun, F.M. Delnick, D.S. Aaron, A.B. Papandrew, M.M. Mench, T. A. Zawodzinski, Probing electrode losses in all-vanadium redox flow batteries with impedance spectroscopy, ECS Electrochem. Lett. 2 (2013) A43–A45, https://doi.org/10.1149/2.001305eel.
[24] A.M. Pezeshki, R.L. Sacci, F.M. Delnick, D.S. Aaron, M.M. Mench, Elucidating effects of cell architecture, electrode material, and solution composition on overpotentials in redox flow batteries, Electrochim. Acta 229 (2017) 261–270, https://doi.org/10.1016/j.electacta.2017.01.056.

[25] T.H. Wan, M. Saccoccio, C. Chen, F. Ciucci, Influence of the discretization methods on the distribution of relaxation times deconvolution: implementing radial basis functions with DRTtools, Electrochim. Acta 184 (2015) 483–499, https://doi.org/10.1016/j.electacta.2015.09.097.
[26] K.W. Wagner, Zur Theorie der unvollkommenen Dielektrika, Ann. Phys. 345 (1913) 817–855, https://doi.org/10.1002/andp.19133450502.
[27] K.H. Shin, C.S. Jin, J.Y. So, S.K. Park, D.H. Kim, S.H. Yeon, Real-time monitoring of the state of charge (SOC) in vanadium redox-flow batteries using UV–Vis spectroscopy in operando mode, J. Energy Storage 27 (2020), 101066, https://doi.org/10.1016/j.est.2019.101066.
[28] D. Zhang, A. Forner-Cuenca, O.O. Taiwo, V. Yufit, F.R. Brushett, N.P. Brandon, S. Gu, Q. Cai, Understanding the role of the porous electrode microstructure in redox flow battery performance using an experimentally validated 3D pore-scale lattice Boltzmann model, J. Power Sources 447 (2020), 227249, https://doi.org/10.1016/j.jpowsour.2019.227249.
[29] H. Schichlein, A.C. Müller, M. Voigts, A. Krügel, E. Ivers-Tiffée, J. Appl. Electrochem. 32 (2002) 875–882, https://doi.org/10.1023/A:1020599525160.
[30] N. Bevilacqua, M.A. Schmid, R. Zeis, Understanding the role of the anode on the polarization losses in high-temperature polymer electrolyte membrane fuel cells using the distribution of relaxation times analysis, J. Power Sources 471 (2020), 228469, https://doi.org/10.1016/j.jpowsour.2020.228469.
[31] J.P. Schmidt, T. Chrobak, M. Ender, J. Illig, D. Klotz, E. Ivers-Tiffée, Studies on $LiFePO_4$ as cathode material using impedance spectroscopy, J. Power Sources 196 (2011) 5342–5348, https://doi.org/10.1016/j.jpowsour.2010.09.121.
[32] T. Tichter, J. Schneider, D. Nguyen Viet, A. Diaz Duque, C. Roth, Rotating ring-disc electrode measurements for the quantitative electrokinetic investigation of the V_3^+-reduction at modified carbon electrodes, J. Electroanal. Chem. 859 (2020), 113843, https://doi.org/10.1016/j.jelechem.2020.113843.
[33] S. Ressel, F. Bill, L. Holtz, N. Janshen, A. Chica, T. Flower, C. Weidlich, T. Struckmann, State of charge monitoring of vanadium redox flow batteries using half cell potentials and electrolyte density, J. Power Sources 378 (2018) 776–783, https://doi.org/10.1016/j.jpowsour.2018.01.006.
[34] M. Skyllas-Kazacos, M. Kazacos, State of charge monitoring methods for vanadium redox flow battery control, J. Power Sources 196 (2011) 8822–8827, https://doi.org/10.1016/j.jpowsour.2011.06.080.
[35] X. Gao, R.P. Lynch, M.J. Leahy, D.N. Buckley, Spectroscopic study of vanadium electrolytes in vanadium redox flow battery (VRFB), ECS Trans. 45 (2013) 25–36, https://doi.org/10.1149/04526.0025ecst.
[36] L. Eifert, R. Banerjee, Z. Jusys, R. Zeis, Characterization of carbon felt electrodes for vanadium redox flow batteries: impact of treatment methods, J. Electrochem. Soc. 165 (2018) A2577–A2586, https://doi.org/10.1149/2.0531811jes.
[37] A.M. Pezeshki, J.T. Clement, G.M. Veith, T.A. Zawodzinski, M.M. Mench, High performance electrodes in vanadium redox flow batteries through oxygen-enriched thermal activation, J. Power Sources 294 (2015) 333–338, https://doi.org/10.1016/j.jpowsour.2015.05.118.
[38] M. Schönleber, E. Ivers-Tiffée, Approximability of impedance spectra by RC elements and implications for impedance analysis, Electrochem. Commun. 58 (2015) 15–19, https://doi.org/10.1016/j.elecom.2015.05.018.
[39] M. Schönleber, D. Klotz, E. Ivers-Tiffée, A method for improving the robustness of linear kramers-kronig validity tests, Electrochim. Acta 131 (2014) 20–27, https://doi.org/10.1016/j.electacta.2014.01.034.
[40] SGL CARBON GmbH, SIGRACELL battery felts - Datasheet company webpage https://www.sglcarbon.com/en/markets-solutions/material/sigracell-battery-felts/ (accessed on 20.08.2022).
[41] Schweiss, R.; Meiser, C.; Damjanovic, T.; Galbiati, I.; Haak, N. SIGRACET® Gas Diffusion Layers for PEM Fuel Cells, Electrolyzers and Batteries. 2016. Available online: https://www.researchgate.net/profile/ (accessed on 20.08.2022).
[42] B. de Mot, J. Hereijgers, M. Duarte, T. Breugelmans, Influence of flow and pressure distribution inside a gas diffusion electrode on the performance of a flow-by CO_2 electrolyzer, Chem. Eng. J. 378 (2019), 122224, https://doi.org/10.1016/j.cej.2019.122224.
[43] M.A. Danzer, E.P. Hofer, Electrochemical parameter identification—an efficient method for fuel cell impedance characterisation, J. Power Sources 183 (2008) 55–61, https://doi.org/10.1016/j.jpowsour.2008.04.071.
[44] J. Schneider, T. Tichter, P. Khadke, R. Zeis, C. Roth, Deconvolution of electrochemical impedance data for the monitoring of electrode degradation in VRFB, Electrochim. Acta 336 (2020), 135510, https://doi.org/10.1016/j.electacta.2019.135510.
[45] N. Roznyatovskaya, J. Noack, K. Pinkwart, J. Tübke, Aspects of electron transfer processes in vanadium redox-flow batteries, Curr. Opin. Electrochem. 19 (2020) 42–48, https://doi.org/10.1016/j.coelec.2019.10.003.
[46] F.H. Rhodes, C.B. Barbour, The viscosities of mixtures of sulfuric acid and water, Ind. Eng. Chem. 15 (1923) 850–852, https://doi.org/10.1021/ie50164a033.
[47] Y. Zhao, Le Liu, X. Qiu, J. Xi, Revealing sulfuric acid concentration impact on comprehensive performance of vanadium electrolytes and flow batteries, Electrochim. Acta 303 (2019) 21–31, https://doi.org/10.1016/j.electacta.2019.02.062.
[48] N. Bevilacqua, L. Eifert, R. Banerjee, K. Köble, T. Faragó, M. Zuber, A. Bazylak, R. Zeis, Visualization of electrolyte flow in vanadium redox flow batteries using synchrotron X-ray radiography and tomography – impact of electrolyte species and electrode compression, J. Power Sources 439 (2019), 227071, https://doi.org/10.1016/j.jpowsour.2019.227071.
[49] M. Nourani, B.I. Zackin, D.C. Sabarirajan, R. Taspinar, K. Artyushkova, F. Liu, I. V. Zenyuk, E. Agar, Impact of corrosion conditions on carbon paper electrode morphology and the performance of a vanadium redox flow battery, J. Electrochem. Soc. 166 (2019) A353–A363, https://doi.org/10.1149/2.1041902jes.
[50] W. Wang, X. Fan, J. Liu, C. Yan, C. Zeng, Temperature-related reaction kinetics of the vanadium(iv)/(v) redox couple in acidic solutions, RSC Adv. 4 (2014) 32405–32411, https://doi.org/10.1039/C4RA04278F.
[51] X. Li, J. Xiong, A. Tang, Y. Qin, J. Liu, C. Yan, Investigation of the use of electrolyte viscosity for online state-of-charge monitoring design in vanadium redox flow battery, Appl. Energy 211 (2018) 1050–1059, https://doi.org/10.1016/j.apenergy.2017.12.009.